PH4201: Advanced Optics Laboratory

Mach-Zehnder Interferometer

Susnata Chattopadhyay*†
22MS077

Indian Institute of Science Education and Research, Kolkata,
Mohanpur, West Bengal, 741246, India.

June 6, 2026

Abstract

In this experiment we attempt to demonstrate the formation of linear fringes, then determine the refractive index of air by analyzing the variation of shift of interference fringes with change in pressure inside the pressure chamber. Finally, by forming circular interference fringes, we will attempt to show that the fringes at each detector are exactly out of phase.

Contents

1 Theory **2**
1.1 The Mach-Zehnder Interferometer . . . 2
1.1.1 Phase Relations and Complementary Outputs . . . 2
1.2 The Lorenz–Lorentz Relation: the microscopic origin of Refractive Index . . . 3
1.3 Determination of Refractive Index of air . . . 4

2 Working Formula **6**

3 Experimental Setup **7**

4 Data Analysis **7**
4.1 Linear Fringes . . . 7
4.2 Calculating n_{air} . . . 8
4.3 Verifying that the circular fringes on the detectors are out of phase . . . 9

5 Conclusion **10**
5.1 Discussion and Sources of Error . . . 10

*www.susnata.com †sc22ms077@iiserkol.ac.in

1 Theory

1.1 The Mach-Zehnder Interferometer

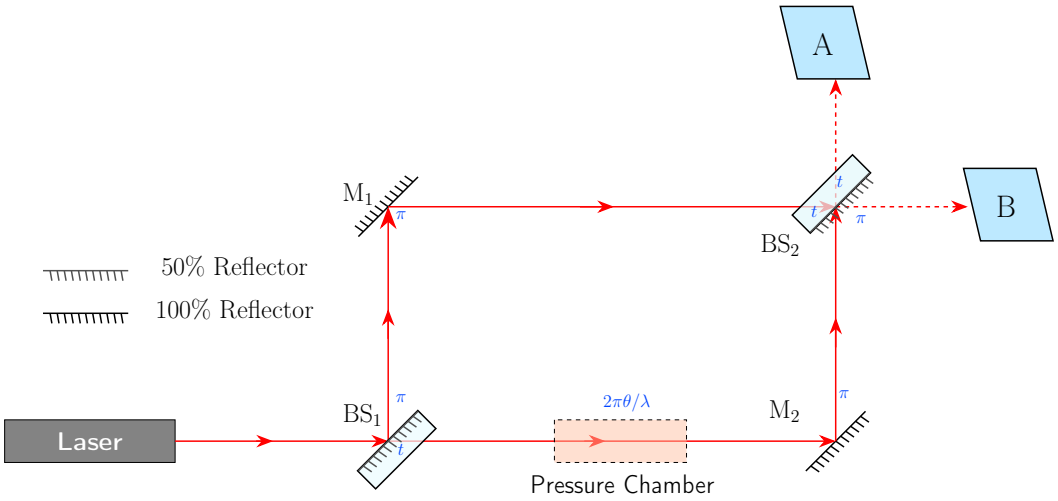


Figure 1: The schematic diagram of Mach-Zehnder Interferometer with a sample of *variable refractive index* in one of the arms.

The Mach-Zehnder interferometer (MZI) is an amplitude-division interferometer (Fig. 1) in which a single coherent beam is split into two spatially separated components using a partially reflecting beamsplitter. These beams propagate along independent paths and are subsequently recombined at a second beamsplitter, producing interference that depends on the relative optical path difference.

A typical arrangement consists of two beamsplitters and two mirrors, directing the beams toward two output screens. Unlike interferometers in which the beams retrace their paths, the MZI allows independent manipulation of each arm. This feature enables the introduction of a controlled optical path difference, for instance by placing a gas cell in one arm, without ambiguity. Let us understand it's working in detail,

1.1.1 Phase Relations and Complementary Outputs

In comparison to the Michelson Interferometer, here each beam traverses a path only once. This results in a more stable interference pattern on the detector, and allows for the insertion of test cells in one of the arms without geometric restrictions.

To begin an analysis of the interferometer, we will first have to note the phase shifts induced by reflections and transmissions, as predicted by the Fresnel equations.

- **Reflection:** If light is incident from an optically rarer medium on a boundary with an optically denser medium, and is reflected at the boundary, the phase shift is given by π. In the opposite case, there is no phase shift.
- **Transmission:** On transmission across a boundary, there is no phase shift accumulated.

In the experiment, we will be using a 50-50 beamsplitter with a dielectric (non-conducting and non-magnetic) coating on only one side. We shall refer to this side as the "reflective side" in the rest of the report. Due to this, the phase shifts induced depend on the face of the beamsplitter that the beam approaches:

- If the beam hits the reflective side from air, there is a phase shift of π. The beam that is transmitted passes through the glass behind the dielectric and is not phase shifted.

- If the beam hits the reflective side from glass, the reflected beam suffers no phase shift. The transmitted beam as usual, passes through the dielectric coating without any phase shift.

To further simplify our analysis, we note that the dielectric coating on the two beamsplitters in the setup are on opposite sides, and that the beam is incident at the same angle at both the beamsplitters. The latter condition ensures that the optical path of beams traversing the beamsplitter material are equal, and that the phase shift accumulated due to that is the same in both arms.

Let us refer to the two beams emerging from the first beamsplitter (BS_1) as shown in Fig. (1) as *upper* and *lower* beams. Let us denote the distance in air travelled by both these beams as l_1 and l_2 respectively. Denote t as the **optical distance** traversed on one crossing of a beamsplitter (for now **do not** consider the presence of the Pressure Chamber). In Table 1 we summarise the net phase accumulated by each of these beams on reaching detectors A and B respectively.

Beam	**Path**	**Phase**
Upper	$\rightarrow BS_1 \rightarrow M_1 \rightarrow BS_2 \rightarrow A$	$\frac{2\pi}{\lambda} l_1 + \pi + \pi + \frac{2\pi}{\lambda} \cdot 2t$
Upper	$\rightarrow BS_1 \rightarrow M_1 \rightarrow BS_2 \rightarrow B$	$\frac{2\pi}{\lambda} l_1 + \pi + \pi + \frac{2\pi}{\lambda} \cdot t$
Lower	$\rightarrow BS_1 \rightarrow M_2 \rightarrow BS_2 \rightarrow A$	$\frac{2\pi}{\lambda} l_2 + \frac{2\pi}{\lambda} \cdot t + \pi + \frac{2\pi}{\lambda} \cdot t$
Lower	$\rightarrow BS_1 \rightarrow M_2 \rightarrow BS_2 \rightarrow B$	$\frac{2\pi}{\lambda} l_2 + \frac{2\pi}{\lambda} \cdot t + \pi + \pi$

Table 1: Phase shifts accumulated by each beam

This makes it easy to calculate the net phase difference between the two beams on reaching

- **Detector A**

$$\Delta\phi_{\mathrm{A}} = \frac{2\pi}{\lambda}(l_1 - l_2) + \pi$$

- **Detector B**

$$\Delta\phi_{\mathrm{B}} = \frac{2\pi}{\lambda}(l_1 - l_2) = \Delta\phi_{\mathrm{A}} - \pi$$

This implies a *constructive* interference at detector B, while *destructive* interference at detector A. Under perfect (ideal) alignment of the beams, we would see a single bright spot at B and darkness at A. However, due to experimental misalignments, some slight angle remains between the beams and consequently causes a fringe pattern.

Since we are using collimated laser source in our experiment, the fringes will appear as parallel non-localized fringes. We place a lens in front of each detector to magnify the interference pattern on the screen (Fig. 3). With the help of markings on the screen, it is possible to count the number of fringes shifted as the optical path traversed by one of the beam changes with respect to the other (i.e when we place the pressure chamber in one of the arms, and vary the pressure inside it ; see Sec. 4.2).

1.2 The Lorenz–Lorentz Relation: the microscopic origin of Refractive Index

The refractive index of a gaseous medium arises from the interaction of electromagnetic radiation with its constituent molecules. When an oscillating electric field $\mathbf{E}$ passes through the medium, it induces a displacement of the electronic charge distribution within each molecule, thereby generating an induced dipole moment,

$$\mathbf{p} = \varepsilon_0 \alpha \, \mathbf{E}_{\mathrm{loc}}, \tag{1}$$

where α denotes the molecular polarizability and $\mathbf{E}_{\text{loc}}$ is the local electric field experienced by the molecule.

The local field differs from the macroscopic field due to the influence of surrounding dipoles. For an isotropic medium, this correction can be evaluated by considering a spherical cavity enclosing the molecule, leading to the Lorentz field expression

$$\mathbf{E}_{\text{loc}} = \mathbf{E} + \frac{\mathbf{P}}{3\varepsilon_0}, \tag{2}$$

In CGS Units, it would have been

$$\mathbf{E}_{\text{loc}} = \mathbf{E} + \frac{4\pi}{3}\mathbf{P},$$

where $\mathbf{P}$ is the macroscopic polarization. Writing $\mathbf{P} = N\mathbf{p}$, with N the number density, yields a self-consistent relation between $\mathbf{P}$ and $\mathbf{E}$:

$$\mathbf{P} = N\varepsilon_0\alpha\left(\mathbf{E} + \frac{\mathbf{P}}{3\varepsilon_0}\right) \tag{3}$$

Solving this expression gives

$$\boxed{\mathbf{P} = \frac{N\varepsilon_0\alpha}{1 - N\alpha/3}\,\mathbf{E}} \tag{4}$$

From Maxwell's equations, the polarization in a non-magnetic medium is also related to the refractive index through $\mathbf{P} = \varepsilon_0(n^2 - 1)\mathbf{E}$. Equating the two expressions leads to the Lorenz–Lorentz relation,

$$\frac{n^2 - 1}{n^2 + 2} = \frac{N\alpha}{3} \tag{5}$$

For practical applications, it is convenient to express this relation in terms of mass density. Using $N = N_A\rho/M$, where N_A is Avogadro's number and M is the molar mass, one obtains

$$R_i \equiv \frac{n_i^2 - 1}{n_i^2 + 2} \cdot \frac{1}{\rho_i} = \frac{N_A\alpha_i}{3M_i} \tag{6}$$

The quantity R_i, known as the **specific refraction** of i-th gas, is independent of density to a good approximation and depends only on molecular properties and wavelength. ρ_i is the partial density of i-th gas.

For a mixture of gases, the total polarization can be expressed as the sum of individual contributions, leading to

$$\boxed{\frac{n^2 - 1}{n^2 + 2} = \frac{N\bar{\alpha}}{3} \equiv \sum_i R_i\rho_i\ ,} \tag{7}$$

where $\bar{\alpha}$ is the mean polarizability of the mixture of gases. Eq. (7) is the fundamental relationship between the refractive index of a gas and its density, and is known as the **Lorentz-Lorenz equation** [1].

1.3 Determination of Refractive Index of air

Air is composed of several gaseous components, the most significant of which are nitrogen, oxygen, water vapor, and carbon dioxide. Since we have no methods available to determine the composition

[1] For a detailed derivation refer to textbook by Borne-Wolf, *Principles of Optics*

of the air in the laboratory, we will be considering air to be a *homogenous* substance with a definite specific refractivity R and density ρ.

Under standard laboratory conditions, the refractive index of air $n \approx 1$. As a result of this, we can make the following approxximation

$$\frac{n^2-1}{n^2+2} = \frac{(n-1)(n+1)}{n^2+2} \simeq \frac{2(n-1)}{3}$$

Substituting these into the Lorentz-Lorentz equation [Eq. 7], the relation simplifies to the **Gladstone-Dale Law**

$$n - 1 \simeq \frac{3}{2} R\rho \tag{8}$$

For simplicity, consider this air cell to behave as an ideal gas. Therefore,

$$\rho \propto P/T \propto (n-1)$$

Hence, one can easily scale the standard conditions (n_0, P_0, T_0) to calculate the experimental conditions (n, P, T).

$$n - 1 = (n_0 - 1)\left(\frac{P}{P_0}\right)\left(\frac{T_0}{T}\right)$$

Since ambient laboratory temperatures remain constant, we may write $T/T_0 \sim 1$ throughout the experiment. When a gas cell of length d (*pressure chamber*) is introduced into one of the arms of the interferometer, any change in pressure (by pumping) alters the refractive index of the medium inside the cell. Let the initial pressure inside the chamber be P_i (correspondingly refractive index n_i). We change it to P_f. Then,

$$n_f - 1 = (n_0 - 1)\left(\frac{P_f}{P_0}\right)$$
$$n_i - 1 = (n_0 - 1)\left(\frac{P_i}{P_0}\right)$$

Substracting the equations yield

$$\boxed{\Delta n = n_f - n_i = \frac{(n_0-1)}{P_0}(P_f - P_i) \implies \frac{\Delta n}{\Delta P} = \frac{(n_0-1)}{P_0} = \text{constant!}} \tag{9}$$

Now, back to our MZI setup. Introduction of this pressure chamber, will add to the path lenghth in one of the beams. Consider a sharp fringe in one of the detectors (say A), since we do not shift any other arrangements of the setup during the process of changing pressure, the original path length ($\Delta x_0 = \Delta\phi_A \lambda/2\pi$; see Sec. 1.1.1) remains **constant**. Then, the condition for the appearance of one of the bright fringe (order m_i) at a location on the screen must be given by[2],

$$m_i\lambda = \Delta x_0 + d(n_i - 1)$$

When we change the pressure, $n_i \to n_f$, thus $m_i \to m_f$ and the **fringe moves** in one direction.

$$m_f\lambda = \Delta x_0 + d(n_f - 1)$$

Substract this two expressions,

$$\boxed{\Delta m \equiv m_f - m_i = \frac{d}{\lambda}(n_f - n_i) = \frac{d}{\lambda}\Delta n}$$

[2] $d(n-1)$ is the extra path length travelled by the beam upon the introduction of the pressure chamber.

This expression can be rewritten using Eq. 9, to get

$$\frac{\Delta n}{\Delta P} = \frac{n_0 - 1}{P_0} = \frac{\Delta m}{\Delta P}\frac{\lambda}{d} \tag{10}$$

Assuming NTP (Normal Temperature and Pressure) conditions in the laboratory, $T_0 = 293.15$ K and $P_0 = 1\text{atm} = 760\text{torr}$, we calculate the refractive index of air $n_0 = n_{\text{air}}$ in this conditions,

$$\boxed{n_{\text{air}} = 1 + \frac{P_0\lambda}{d}\frac{\Delta m}{\Delta P}} \tag{11}$$

2 Working Formula

Notice that, in Eq. 11, both Δm and ΔP are variables, and they are linearly related to each other. So in principle we can plot Δm v/s ΔP for multiple such readings and linear fit it (as explored in Sec. 4.2) to obtain the slope and intercept,

$$\Delta m = (\text{slope}) \times \Delta P + (\text{intercept}) \simeq (\text{slope}) \times \Delta P$$

since magnitude of intercept $\ll 1$, we can easily neglect it. Thus, we calculate the n_{air} by the following formula

$$\boxed{n_{\text{air}} = 1 + \frac{P_0\lambda}{d} \times \text{slope}\left(\frac{\Delta m}{\Delta P}\right) \equiv 1 + \frac{P_0\lambda}{d}s}$$

In the present experiment, $\lambda_0 = 655\,\text{nm}$ and $d = (8.0 \pm 0.1)\,\text{cm} = 8 \times 10^7\,\text{nm}$.

3 Experimental Setup

Our experimental setup (Fig. 2) of Mach–Zehnder interferometer consists of the the following components: a coherent laser source ($\lambda = 655\,\text{nm}$), two 50:50 beam-splitters, 2 plane mirrors on adjustable kinematic mounts, a pressure chamber of fixed length ($d = 8\,\text{cm}$), Barometer for pressure measurement, 2 plano-convex/convex lenses, Optical table, screws, and screw driver, and cardboard Screen (or detector) for observing interference fringes.

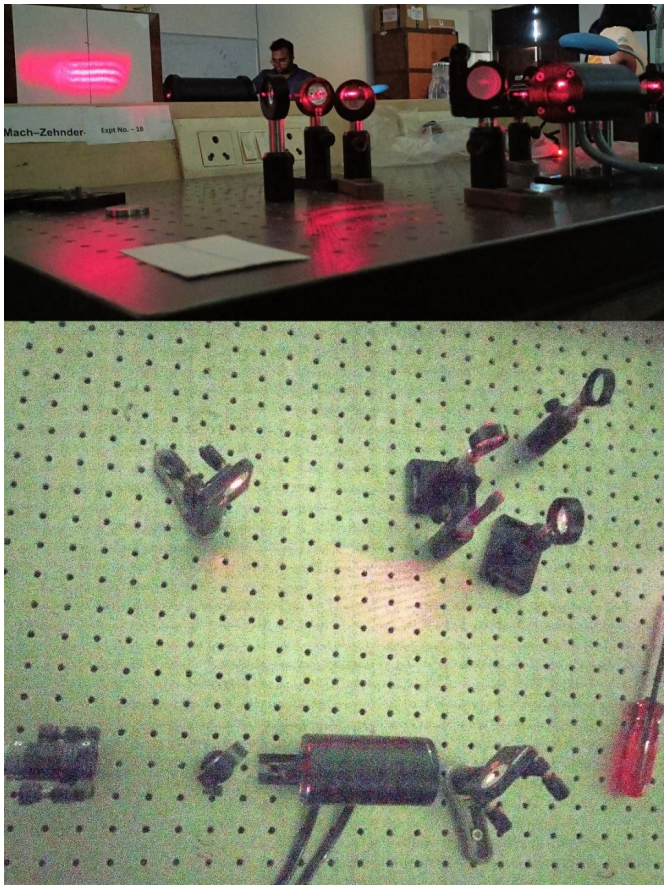


Figure 2: The setup at the laboratory

4 Data Analysis

4.1 Linear Fringes

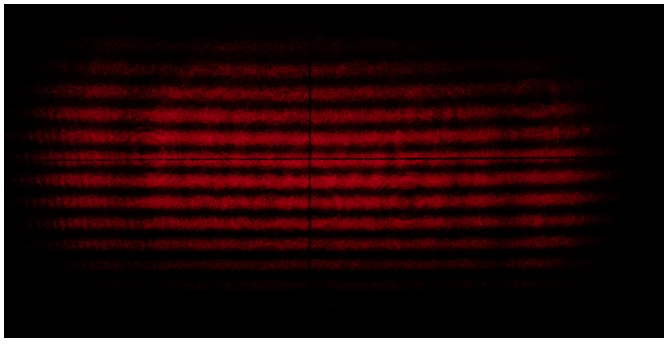


Figure 3: We obtain straight fringes from the interference of beams with planar wavefront. The sharper of the two fringes is shown here for clarity.

The interferometer is first aligned so that linear interference fringes are visible on both screens [Fig. 3]. We note that the contrast of the fringes differs between the two screens. This is because, the intensities of the interfering beams are not the same, and the beam splitter used is **not an ideal** (50:50) beam splitter. As a result, the contrast on one screen is lower than on the other.

4.2 Calculating n_{air}

In the later part of the analysis, we consider only the screen with better contrast. By placing a pressure chamber along one of the arms, we can vary the path length by varying the pressure. This results in a fringe shift observed on the screen. We obtain the data for number of fringes shifted (Δm) vs Pressure in chamber (P in mmHg) for 3 different sets of measurements [Table 3]. The recorded data points and their corresponding linear fits are plotted in Figure 4.

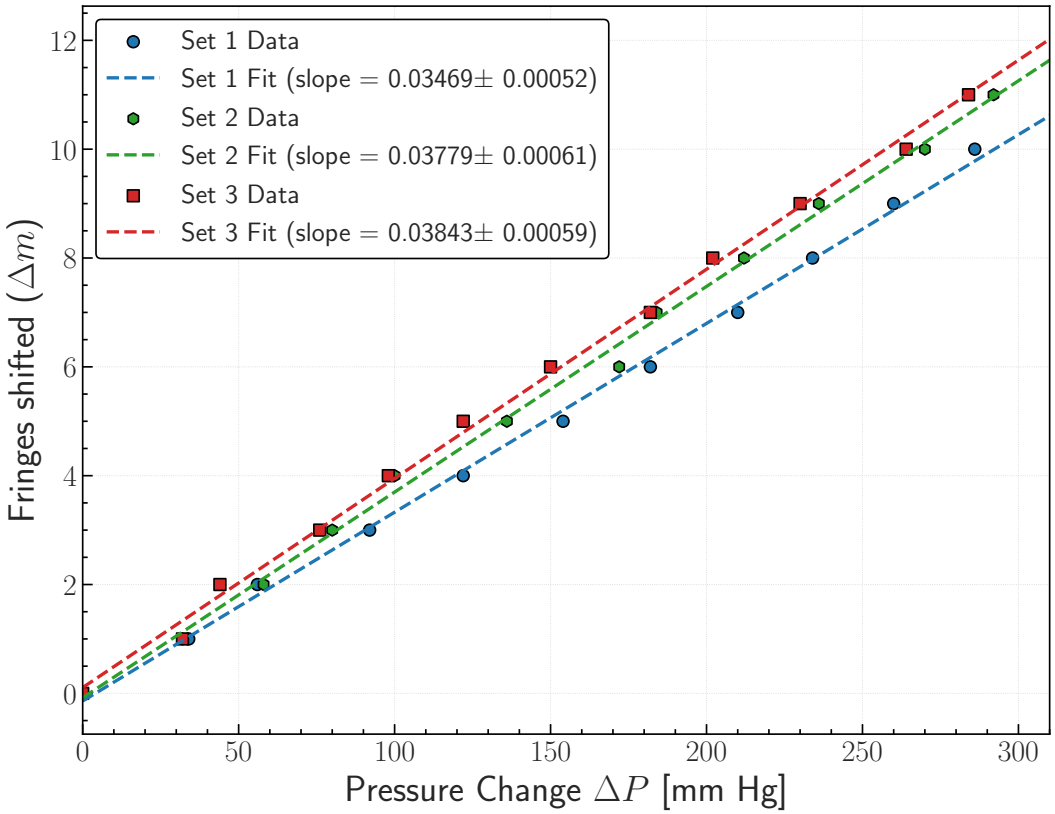


Figure 4: Linear fit of fringe shift (Δm) versus pressure difference (ΔP) for three independent trials.

Note that (as plotted in the Fig. 4 above), the Y-axis ΔP corresponds to

$$\Delta P = P_{\Delta m} - P_{(\Delta m=0)}$$

A linear curve fit was applied to each dataset to extract the rate of fringe shift with respect to pressure, defined by the slope $s = \text{slope}\left(\frac{\Delta m}{\Delta P}\right)$. The extracted slopes for the individual trials and their arithmetic mean are summarized in Table 2.

Set	s (mmHg^{-1})	δs (mmHg^{-1})
Set 1	0.034695	0.000525
Set 2	0.037792	0.000611
Set 3	0.038433	0.000589

Table 2: Extracted slopes and linear fit errors from the experimental data

Taking the arithmetic mean of the three trials, the average slope is calculated to be

$$\bar{s} = 0.036973 \text{ mmHg}$$

We then use the working formula to calculate the refractive index of air at NTP conditions,

$$\begin{aligned} n_{\text{air}} &= 1 + \bar{s}\left(\frac{P_{\text{atm}}\lambda}{d}\right) \\ &= 1 + 0.036973 \times \left[\frac{760 \times (655 \times 10^{-9})}{8.0 \times 10^{-2}}\right] \\ &= 1 + 0.036973 \times 6.2225 \times 10^{-3} \\ &= 1.000230064 \end{aligned}$$

Error Analysis We have,

$$n_{\text{air}} = 1 + \bar{s}\left(\frac{P_{\text{atm}}\lambda}{d}\right)$$
$$\therefore \left|\frac{\Delta n_{\text{air}}}{n_{\text{air}}}\right| \leq \left|\frac{\Delta \bar{s}}{\bar{s}}\right| + \left|\frac{\Delta d}{d}\right|$$

$\Delta\bar{s}$ is calculated using the formula,

$$\Delta\bar{s} = \frac{1}{3}\sqrt{(\delta s_1)^2 + (\delta s_2)^2 + (\delta s_3)^2} = 3.32643 \times 10^{-4}$$

Hence,

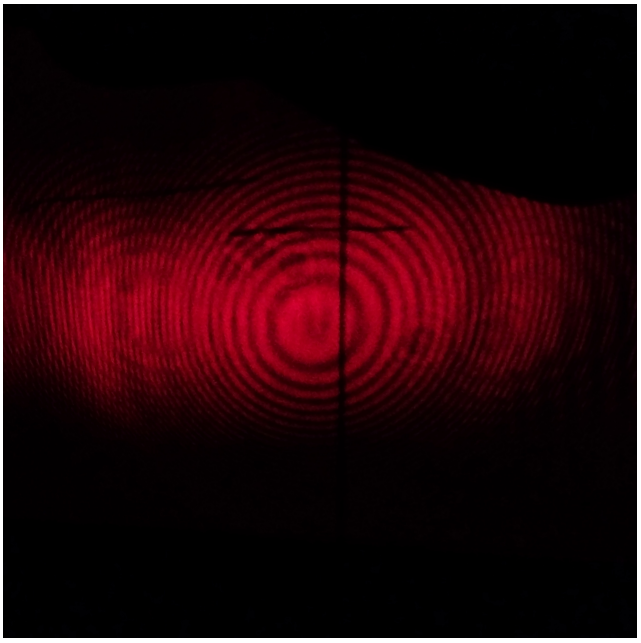
$$\begin{aligned} |\Delta n_{\text{air}}| &\leq n_{\text{air}} \times \left[\frac{3.32643 \times 10^{-4}}{0.036973} + \frac{0.1}{8}\right] \\ &= 0.021502 \end{aligned}$$

Hence, we report our experimentally measured value as

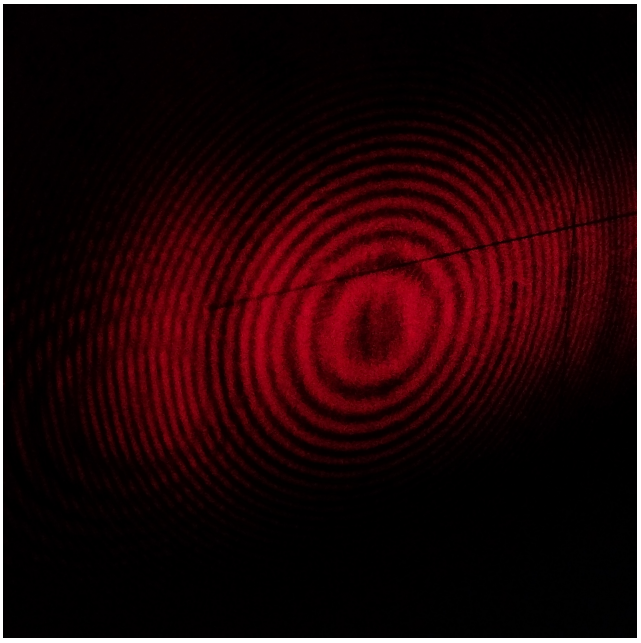
$$\boxed{n_{\text{air}} = 1.000230 \pm 0.021502}$$

4.3 Verifying that the circular fringes on the detectors are out of phase

When a lens is inserted in front of the collimated beam from the laser (in one of the arms), the plane wave becomes a diverging spherical wave. Thus, circular fringes are produced due to the interference of these spherical wavefronts, which are depicted in the figure below. The central spot is maximum (bright spot) in one path [Fig. 5a] and minimum (dark spot) in the other [Fig. 5b]. Hence, we successfully demonstrate that the beams projected on the two screens have a phase difference of π.



(a) Central bright fringe



(b) Central dark fringe

Figure 5: Complementary Circular Fringes obtained in our experiment

5 Conclusion

The refractive index of air was determined to be 1.000230 ± 0.021502. Spherical fringes were obtained, and a successful demonstration of the complementary nature of the center spot was shown.

5.1 Discussion and Sources of Error

Since the refractivity of air is of the order of 10^{-6}, this experiment is highly sensitive and prone to both random and systematic errors. The major sources of uncertainty are discussed below.

- The first and foremost error comes from the assumption of temperature of the laboratory, which we assumed to be $\simeq T_0 = 25°\text{C}$.
- Adiabatic heating: Introducing air into the pressure cell causes compression, which leads to adiabatic heating of the enclosed air. As a result, the temperature inside the cell may differ from the ambient room temperature, affecting the measurement. To reduce this effect, the pressure was held constant at each step until the fringe pattern became visually stable.
- Window deformation: Increasing the pressure inside the cell creates a pressure difference across the windows, which may cause slight bending. This can make the windows behave like weak meniscus lenses, thereby reducing the effective optical path length and slightly distorting the collimated beam. Such distortion may introduce curvature in the otherwise straight fringes, leading to errors in fringe shift measurements.
- Changes in air composition: The local composition of air in the laboratory may vary during the experiment. For instance, breathing near the setup can increase the concentration of carbon dioxide and water vapour. Since these constituents have different refractivities, such fluctuations can introduce errors in the calculated refractive index.
- Geometrical misalignment: Imperfect alignment of the optical components along the beam path can result in lateral and angular beam deviations. Although the interferometer is

relatively tolerant to small lateral displacements, larger angular misalignments can reduce fringe contrast on the detector screen, thereby affecting measurement accuracy.

- Fringe counting uncertainty: The most significant source of error in this experiment arises from uncertainty in counting fringe shifts. A more accurate and conservative estimate of this uncertainty could be obtained by using an electronic detection system to monitor changes in fringe contrast.
- Secondary reflections: Weak reflections from the glass surfaces of optical components may produce secondary interference fringes superimposed on the primary pattern. This reduces fringe contrast and makes it more difficult to identify the fringe center accurately. Careful alignment and adjustment can help minimize this effect. In addition, dust or greasy surfaces on optical elements can further enhance such unwanted reflections.

References

- Lab Manual

Appendix

Δm	Set 1 (mmHg)	Set 2 (mmHg)	Set 3 (mmHg)
0	6	6	6
1	40	38	38
2	62	64	50
3	98	86	82
4	128	106	104
5	160	142	128
6	188	178	156
7	216	190	188
8	240	218	208
9	266	242	236
10	292	276	270
11	-	298	290

Table 3: The three sets of pressure readings inside the pressure chamber, as we observe a unit shift in interfernce fringes (Δm)